

# Computer-Assisted Path Planning for Minimally Invasive Vascular Surgery

HUANG Dongjin<sup>1,2</sup>, TANG Pengbin<sup>1</sup>, WANG Yin<sup>1</sup>, LI Hejuan<sup>1</sup>, TANG Wen<sup>3</sup> and DING Youdong<sup>1,2</sup>

(1. Shanghai Film School, Shanghai University, Shanghai 200072, China)

(2. Shanghai Engineering Research Center of Motion Picture Special Effects, Shanghai 200072, China)

(3. Department of Creative Technology, University of Bournemouth, Fern Barrow, Poole BH12 5BB, UK)

**Abstract** — Path planning assisted by two-dimensional medical images is an essential part of minimally invasive diagnosis and treatment for cardiovascular diseases. Due to the complex background of angiography images and vascular structure with multi-branch and stenoses, creating accurate pathways from angiography image is a challenge task. In this paper, we present a new path planning methodology based on angiography medical images using the steady fluid dynamics. Our novel approach is useful in many medical applications, such as for computer-assisted medical images analysis and the follow-on image-guided interventions. A graph-cuts based energy function was applied to the vessel segmentation of angiography images in order to obtain boundary information. We have adopted Finite Volume Method (FVM) to simulate the Newtonian fluid inside the segmented blood vessels, and a set of isobars under the steady fluid condition are obtained by Meandering Triangles algorithm. The selected center points of isobars are organized to generate the directed vessels-tree, from which the vascular stenoses are automatically detected and the final surgical path is generated with branches. Our method can be used for quantitative path analysis, and we show experimental results to demonstrate that the versatile and applicability of the algorithm in obtaining single-pixel surgical path with good performance, high accuracy and less manual interventions, especially it is robust on complex vascular structures.

**Key words** — Minimally Invasive Surgery, Path planning, Fluid dynamics, Medical Images Analysis.

## I. Introduction

X-Ray/CT images are common image modality for preoperative planning, including the selection of operative methods, procedures and approaches. Guidewire path planning is an important pre-operative procedure

in minimally invasive surgery for cardiovascular diseases. Path planning can reduce potential surgical injury such as damage to adjacent tissues during guidewire insertions, thus, improving the accuracy of lesion localization and the success of surgery. The surgical path is often expressed by blood vessels centerlines. Therefore, efficient and accurate extraction of vascular centerlines is a core computational process for minimally invasive vascular surgery.

There are three impediments that make it difficult to extract the centerline of human blood vessels accurately: 1) It is hard to perform vessel segmentation from angiography sequences of low image quality with complex background. A fully automatic way of blood vessel segmentation is still challenging; 2) Blood vessels are complex tree like structures that have many small sub-branches. Especially, vascular stenosis and occlusion do exist in disease vessels that make the internal structure of the vessels even more complex; 3) Traditional centerline extraction algorithm usually require manual interventions in order to adjust the extraction results to achieve high accuracy. This causes low computational efficiency and low accuracy.

To address these problems, in this paper, we propose a novel method for efficient and accurate centreline extraction. Our method is based on a two-stage approach. Firstly, image preprocess is performed by using the Graph-cuts based 2D blood vessels segmentation method for angiography images [1]. Secondly, by analysing the isobars of steady fluid inside tube shaped objects i.e. blood vessels, we discover the correlation between the center positions of isobars with the center of tube shaped structure. Based

\*Manuscript Received July XX, 2017; Accepted July XX, 2017. This work is supported by the National Natural Science Foundation of China (No.61402278), the Shanghai Natural Science Foundation of China (No.14ZR1415800), the Innovation Program of the Science and Technology Commission of Shanghai Municipality of China (No.16511101302) and 2016 Shanghai University the peak discipline of filmology.

on this novel approach, we apply hydrodynamics computation inside in the blood vessel structure for centerline extraction and propose a new path planning algorithm based on steady fluid dynamics. This algorithm calculates the isobars under steady fluid by presetting the inlet and outlet boundaries, constructs the directed tree with flow velocity to detect the vascular stenoses automatically and fits a continuous and smooth surgical path with several branches by Catmull-Rom spline. Finally, we set four different kinds of experiments to validate the accuracy of centerline extraction and rate of stenoses, and use this algorithm to obtain the surgical path from 2D medical CT angiography images with good experimental results. Our algorithm requires little manual intervention and could extract a smooth and single-pixel surgical path accurately. Further more, it is not only suitable for 2D models, but also can be easily expanded to 3D objects, such as tubular structures (like bile duct, colon, etc), multi-branch objects (like tree, vein, etc) and so on.

## II. Related work

The surgical path built from medical images includes the information of blood vessel profile, branch points, width, centerline and stenoses locations, which is the core surgical evidence for cardiovascular disease diagnostic and treatment. In this section, we first review centerline extraction methods for blood vessels, then highlight the related medical applications on path planning.

Centerline, known as skeleton or medial axis, is established by the foundation of skeletonization in the form of medial loci of an object in  $R^n$  that forms the skeleton of the object with the features of connectivity, centrality and unicity [2]. In the field of vascular centerline extraction, a number of algorithms have been proposed and applied in the angiography images recently. The centerline of blood vessels is considered as a ridge formed by a series of ridge points. Based on the ridge points, Shoujun et al. [3] and Cruz-Aceves et al. [4] applied Gabor filter on extracting the centerline of blood vessel. Although those algorithms have high precision, they need to track the vascular tendency thus cannot do automatically. Krissian et al. [5] and Staal et al. [6] proposed the vascular centerline extraction algorithm based on multi-scale method. The center point obtained by this gray level distribution-based method is consistent with human vision, but the scale selection has greatly influenced the extraction result.

In the recent years, the method of topological thinning algorithm, distance transform algorithm and Voronoi diagram methods have been gained widely attention. In the topological thinning strategy, Au et al. [7] obtained 1D skeletal shape by performing geometry contraction using constrained Laplacian smoothing. Wang et al. [8] it-

eratively contract the mesh of blood vessels and subdivide the contracted mesh to point cloud, then a skeleton growing procedure is employed for generating the curve skeleton. And Wu et al. [9] also proposed a topological thinning method to plan the flight path of endoscopic camera and hierarchy vessel labeling. In this method, one layer at a time of voxels is peeled off the object until just the skeleton remains. Unfortunately, because of the complex topological information of vascular, topological thinning algorithm is computationally expensive. For distance transformation algorithms, Liu et al. [10] adopted the performance advantage of GPU to parallel compute the centerline based on distance mapping. Hernandez-Vela et al. [1] segmented the blood vessels from the 2D angiography images and used the segmented vascular for extracting its centerline by distance map. Jin et al. [11] used a minimum cost path approach to extract the centerline of 3D tree-like objects. This kind of method is based on the feature that centerline is the furthest from edges with fast extraction speed. But the centerline is hard to assure only one-pixel and the corner may appear in the blood vessels with big curvature. And Voronoi diagram methods [12][13][14] use the Voronoi diagram of boundary points of objects to obtain its skeleton. This algorithm is suitable for the simple shapes but not the complex structure of human vascular.

Centerline extraction method as a key part has been applied to different medical imaging applications, including path planning [15][16], stenosis detection [17][18], anatomic labeling [19][20], feature extraction [21][22], etc. In this paper, we mainly focus on path planning and stenosis detection. Path planning is a essential step before preoperative planning, there already have path planning applications for bronchoscopy [15] and colonoscopy [16]. Kiraly et al. [15] have computed a set of 3-D airway-tree paths from bronchoscopy MDCT images and used the generated paths for airway analysis and smooth virtual navigation. Kang et al. [16] proposed a view position and corresponding view direction optimization method to minimize the blind areas for accurate diagnosis of colonic polyps. Pan et al. [23] proposed a 3D anatomical structures based discrete potential field algorithm, this method planned the needle surgical path within 3D anatomical soft tissues in minimally invasive surgery. However, there are still few method for path planning of minimally invasive vascular surgery in 2D angiography images. Quantification of coronary arterial stenoses is useful for the diagnosis of several coronary heart diseases, Xu et al. [17] presented a fuzzy distance transform (FDT) method for detecting and quantifying coronary arterial stenosis in computed tomographic angiography. Eslami et al. [18] proposed using cross-sectional area and intensity profile of segmented lumen for quantification of stenosis with sub-

pixel accuracy.

Different from the above algorithms, we utilize the feature of isolars under the steady fluid and design a novel method to extract the centerline of blood vessels

with high accuracy and less inventions, and the stenoses of blood vessel are automatically detected for the following generation of surgical path, which could overcome the shortcomings of traditional approaches described above.

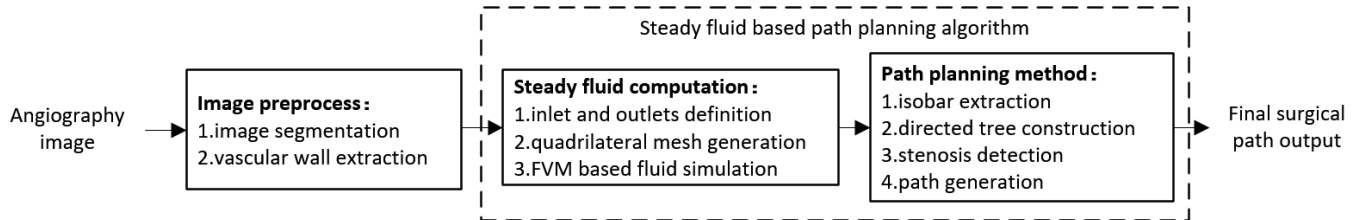


Fig. 1. Block diagram of Path Planning Method

### III. METHOD

#### 1. Method Overview

Fig. 1 depicts a block diagram of the proposed path planning method. In our method, an angiography image is adopted as the input for its following surgical path analysis and generation. Firstly, the preprocess of angiography image should be done to extract the main vascular wall in this image, including image segmentation and vascular wall extraction. Secondly, after definition the inlet and outlets of this vascular, we adopt the paving method for the generation of quadrilateral mesh inner this vascular, and the FVM based fluid method iteratively executes over this meshed vascular until the pressure of fluid tends to stable. Thirdly, we extract the isobar inside of blood vessels based on the steady fluid for generating the vascular directed tree, and detect the position and rate of stenoses in the vascular by the flow velocity variation of directed tree nodes. Then the surgical path is generated from the tip of catheter to the stenoses locations. Finally, the final angiography image is represented to surgeons with the information of surgical path, location and rate of stenoses, branch nodes and so on.

#### 2. Method Details

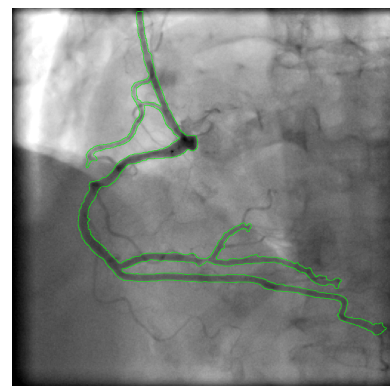
##### (1) Vascular wall extraction

Accurate extraction of vascular wall is a essential step for the path planning of 2D angiography images. We adopt the Graph-cuts based blood vessels segmentation method [1] to automatically obtain accurate blood vessel's wall of the images. Following is the brief description of the method.

In order to achieve automatic segmentation of blood vessel, the initial seeds in the blood vessels are determined by the inherent structure of vessels based on valleys, and background seeds are found based on low probabilities of the vesselness image. Since we adopt the Graph-cuts based method to segment the blood vessel from angiography images, we need to determine the unary term and



(a)



(b)

Fig. 2. Segmentation result [1]

boundary term of images. Therefore, after the initialization of seeds, we define the unary term by exploiting geodesic paths among vessel seeds and using geodesic distance to correct the potential vessel region. And an image-dependent multi-scale edgeness measure is adopted to determine the potential boundary. Then, the min-cut method is adopted to obtain the segmentation with minimum energy, and only the biggest connected component is kept in the final segmentation. Finally, we can easily use the segmentation result to extraction its corresponding vascular wall for the following path planning. The

original angiography image is shown in Fig.2(a), and the corresponding vascular wall is extracted in Fig.2(b).

In the angiography images, the catheter always appears at the beginning of the blood vessels and it is hard to distinguish from arteries. After generated the directed tree in the following parts, we use the directed tree nodes for catheter detection based on multiscale stacked sequential learning method and cut the tree nodes of catheter part in the beginning of the tree.

## (2)Steady fluid computation

### • Navier-Stokes control equation

Because of rheological property of fluid, blood flow in the blood vessels is approximately considered as Newtonian fluid and its viscosity factor is treated as a constant [24]. Therefore, the viscous incompressible Navier-Stokes (N-S) equation is introduced to simulate the dynamics of blood flow in the vessels. And its two-dimensional continuity and momentum equations are:

$$\frac{\partial}{\partial x}(\rho uu) + \frac{\partial}{\partial y}(\rho vu) = \frac{\partial}{\partial x}(\mu \frac{\partial u}{\partial x}) + \frac{\partial}{\partial y}(\mu \frac{\partial u}{\partial y}) - \frac{\partial p}{\partial x} \quad (1)$$

$$\frac{\partial}{\partial x}(\rho uv) + \frac{\partial}{\partial y}(\rho vv) = \frac{\partial}{\partial x}(\mu \frac{\partial v}{\partial x}) + \frac{\partial}{\partial y}(\mu \frac{\partial v}{\partial y}) - \frac{\partial p}{\partial y} \quad (2)$$

$$\frac{\partial}{\partial x}(\rho u) + \frac{\partial}{\partial y}(\rho v) = 0 \quad (3)$$

Where  $u, v$  are horizontal and vertical velocity components of fluid flow respectively;  $p, \rho, \mu$  are pressure, density and viscosity coefficient of the fluid respectively.

Let the vascular wall  $\Gamma$  be a Lipschitz continuous boundary, the fluid satisfies the no-slip condition at the boundary, in other words, the fluid velocity is zero  $u_\Gamma = 0$  relative to the boundary. In the initial phase, we set the velocity direction of inlet fluid as the direction of perpendicular to the inlet boundary and the outlet pressure is set as 0.

### • The finite volume method

The most common computation numerical methods are Eulerian grid based, which mainly including three methods: (1) Finite Difference Method (FDM); (2) Finite Element Method and (FEM); (3) Finite Volume Method (FVM). FDM is easily understood with high efficiency, but lack accuracy. Compared with FDM, FEM can be suitable for complicated shape with high precision, but has high computational complexity and bad real-time performance. FVM is a combination of the above methods, which is suitable for fluid simulation with irregular grid.

Therefore, we adopt the FVM to discretize the control equation. And its basic idea is dividing the computational domain into several non-overlapping control volumes around each node of grids, and integrating each control volumes to obtain a discrete set of equations.

To solve the momentum equations by FVM, we adopt the method of paving to generate quadrilateral mesh according to the complex boundary of blood vessels, as shown in Fig.3. For keeping the precision of computational results, the more refined meshes are distributed nearing the vessel walls.

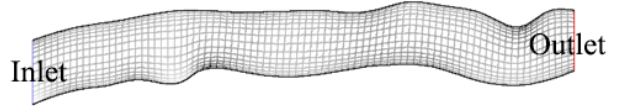


Fig. 3. Mesh generation on the blood vessels

Then, the staggered grid method is adopted for computing the pressure and velocity on the meshed space. That is, the evaluation of pressure is computed at original node of quadrilateral mesh and the evaluation of velocity is calculated on the center staggered grids. As shown in Fig.4, the control volume of node P is u-cell and v-cell in horizontal and vertical direction separately, where  $I, J$  the grid lines (the bold line) and  $i, j$  the cell edges (the dashed line).

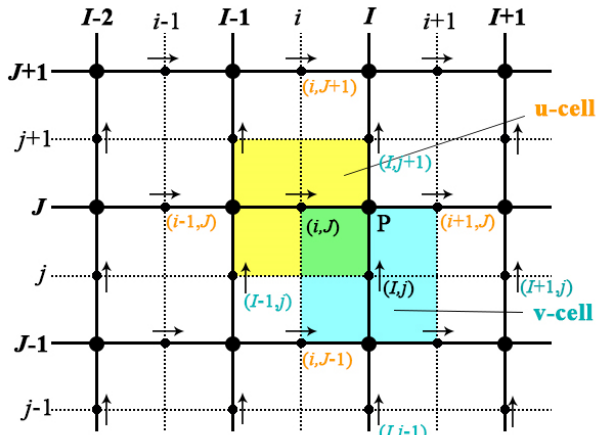


Fig. 4. u and v-control volume of node P and their neighboring velocity components

The velocity components at the intersection of the grid lines and cell edges are calculated by u-cell and v-cell respectively: velocity  $u$  at point  $(i, J)$  is calculated by the discretized u-momentum equation (4); similarly, velocity  $v$  at point  $(I, j)$  is calculated by the v-momentum equation (5).

$$a_{i,J}u_{i,J} = \sum a_{nb}u_{nb} + (P_{I-1,J} - P_{I,J})A_{i,J} \quad (4)$$

$$a_{I,j}v_{I,j} = \sum a_{nb}v_{nb} + (P_{I,J-1} - P_{I,J})A_{I,j} \quad (5)$$

Where  $A_{i,J}$  and  $A_{I,j}$  the length of cell edges;  $a_{i,J}$ ,  $a_{I,j}$  and  $a_{nb}$  the fluid coefficients can be calculated by the differencing methods suiting for steady Navier-Stokes problem;  $\sum a_{nb}u_{nb}$  the summation of u-velocity at  $(i-1, J)$ ,  $(i+1, J)$ ,  $(i, J-1)$  and  $(i, J+1)$ ;  $\sum a_{nb}v_{nb}$  the summation of v-velocity at  $(I, j+1)$ ,  $(I+1, j)$ ,  $(I, j-1)$  and  $(I-1, j)$ .

---

**Algorithm 1**


---

**Require:** Initial guessed pressure fields  $P^*$ .

**While**  $\Delta P < P_\epsilon$  :

1. solve discretized momentum equations (4)(5) to yield velocity components  $u^*$  and  $v^*$ ;
2. solve pressure correction equation deduced from the continuity equation(3) to obtain the correction  $P'$ ;
3. correct pressure and velocities;
4. solve all other discretized transport equations;
5. judge the convergence of velocity and pressure fields;

**End while**

---

In the N-S partial differential equations, the independent variables velocity and pressure are coupled and influence each other. Therefore, the pressure field initialized by guessed pressure field according to the boundary conditions, and the pressure is set as  $P = P^* + P'$ , where  $P^*$  the guessed pressure,  $P'$  the correction pressure. Substituting the guessed pressure  $P^*$  into equation (4)(5) to obtain guessed velocity  $u^*$ ,  $v^*$  and iteratively compute the pressure until the difference  $\Delta P$  between two pressure results continuously less than a constant threshold value  $P_\epsilon$ . The pressure calculation process as Algorithm 1.

### (3)Path planning method

#### • Isobars extraction

The features of isobars is well correlated with the center of blood vessels under steady fluid. So the isobars should be obtained accurately for the further extraction of surgical path. Following Delaunay triangulation and isobars calculation steps are adopted for the extraction of isobars.

Delaunay triangulation: We triangulate the entire irregular grids by Delaunay triangulation and use these triangles for the generation of isoline, because it is hard to obtain the isoline from the irregular quadrilateral grid which their corresponding pressure values are not coplanar.

Isobars calculation: From the previous step, the irregular girds are transferred to triangles. Then, we equally divide the fluid pressure value into the  $n$  levels and adopt Meandering Triangles algorithm to generate isobars for every pressure level.

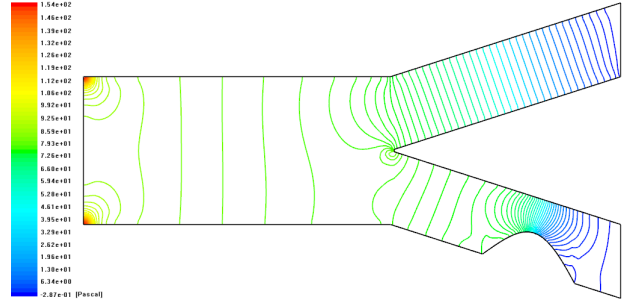


Fig. 5. Isobar extraction

Taking Y-type pipe containing branches and stenosis as an example, the isobars under steady fluid condition is obtained by the method above. As shown in Fig.5, a set of isobars with different colors and pressure is ranked orderly inside the pipe from inlet to outlets.

#### • Surgical Path generation

After getting a set of isobars, we propose a surgical path generation algorithm based on Catmull-Rom spline to generate a smooth and single-pixel path to the leisure part of blood vessel. The whole process is as follows:

##### Step 1: The center points of isobars calculation

Using iterative approximation from both sides of the isobars to compute the center points, which are set as the feature nodes of centerline.

##### Step 2: The directed tree construction

By setting the inlet and outlet pressure, we utilize the characteristic of steady fluid, the pressure generally decreasing from inlet to outlet, to construct the directed tree of the feature nodes.

The head node of directed tree is determined by inlet position and pressure. If multiple nodes are detected, we set them as the head node of different braches respectively. Then, we build the directed tree successively by the descending order of pressure and the proximity principle from these head nodes.

When building the child node of the current with pressure  $P_m$ , we search its child node by pressure  $P_{m-1}$ . If  $k$  nodes were found, then calculating the distances  $d_1, d_2, \dots, d_k$  between current node and these nodes, and taking the node whose distance  $d$  meeting  $d \leq d_{min} + d_e$  as the child node, where  $d_{min} = \text{Min}(d_1, d_2, \dots, d_k)$  is the minimum distance,  $d_e$  is a distance threshold.

##### Step 3: The feature nodes correction

The generated directed tree from step 2 may have some error nodes or miss some nodes. So feature nodes correction is required.

1) Inlet tree correction: the problem of multiple branches at inlet. We correct the head node of directed tree by merging branch nodes. As shown in Fig.6, there are two branches at inlet and they finally connect to a combination point(the red), we merge the same pressure nodes among these branches as the new nodes(the blue),

whose position is the center of the two corresponding ones.

2) Tree branch correction: The problem that the leaf node position does not match the outlet position, we use the directed tree pruning method to ensure that the leaf node is at the outlet. As shown in Fig.6, the pink node is the leaf but not matches the outlet, so this branch needs to be cut.

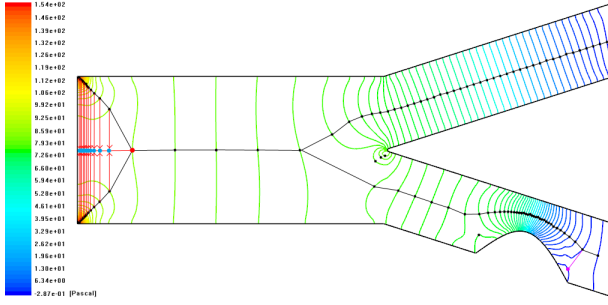


Fig. 6. The construction of directed tree

3) Outlet branch supplement: The problem that the number of leaf nodes less than the number of outlets, we adopt the method of recursive searching parent node to reconstruct the new branches of directed tree.

Firstly, we set the nearest node from outlet which is not constructed as the outlet node. Then, we recursively search the parent node within the range  $d_f = d_{f_{min}} + d_{f_e}$  by ascending order of pressure from this outlet node, where  $d_{f_{min}}$  is the distance to the nearest node within the searching range,  $d_{f_e}$  is the extended distance of the searching range. And there are three conditions to process the nodes within the searching range:

a) If only one node in  $d_f$ , we set this node as the parent of searching node directly.

b) If multiple nodes in  $d_f$  without the parent or the child, we set the nearest one among them as the parent of searching node.

c) If multiple nodes in  $d_f$  and part of them have the parent or the child, we set the nearest one having the parent or the child as the parent of searching node.

**Step 4:** Stenoses detection by variation of flow velocity

The blood flow will vary throughout the stenosis and the variation of blood flow is related to the width of blood vessel due to the Bernoulli law, therefore, we adopt this idea to detect the location of stenoses and compute their corresponding rate of stenosis.

Firstly, we scan the entire directed tree nodes to obtain the stenoses of the blood vessels. In this process, if the velocity (fluid flow) of scan node satisfies  $V_{scan} > \text{Each}\{V_{k_1}^+, \dots, V_1^+, V_1^-, \dots, V_{k_1}^-\}$  and slopes satisfy  $\text{abs}(K_{k_1}^+) > K_{th1}$  and  $\text{abs}(K_{k_1}^-) > K_{th1}$ , we then define this scan node as a stenosed node. Where  $V_{k_1}^+$  and  $V_{k_1}^-$  ( $k_1 = 5$ ) are the velocity of  $k_1$ -th latter and  $k_1$ -th former node of scan node respectively,  $K_{k_1}^+$  and  $K_{k_1}^-$  are the slopes

of  $k_1$ -th latter and  $k_1$ -th former node to scan node, and  $K_{th1}$  is the threshold of the slope.

After defined the stenosed nodes of the directed tree, we then need to obtain the velocity of inlet and outlet of stenosis to determine the rate of stenosis for every stenosed node. We forward and backward seek satisfying nodes from the  $k_1$ -th former and  $k_1$ -th latter node of stenosis node as the inlet and outlet of stenosis respectively, and its rule is (we use the former seeking as an example and the latter seeking is the same.):

1) If the number former nodes from seeking node are less than  $k_2 = k_1/2$ , then the headmost node is set as the inlet of the stenosis; else (2).

2) If the slop of  $k_2$ -th latter node to  $k_2$ -th former node of seeking node  $K_{k_2^+ - k_2^-} < 0$ , then the  $k_2$ -th latter node is set as the inlet of the stenosis; else (3).

3) If  $K_{k_2^+ - k_2^-} < K_{th2}$ , then the  $k_2$ -th latter node is set as the inlet of the stenosis; else (4).

4) If  $K_{k_2^+ - k_2^-} \geq K_{th2}$ , then continuously seeking the former nodes by this rule.

Finally, we compute the rate of stenoses according to the Bernoulli law. The velocity of inlet and outlet of stenosis may exist large difference under different condition. Therefore, if  $\text{abs}(V_{in} - V_{out}) > th3$ , we directly use the slower velocity to compute the stenosis rate as  $P_s = 1 - V_{smaller}/V_{stenosis}$ , where  $V_{in}$ ,  $V_{out}$  and  $V_{stenosis}$  are the velocity of inlet, outlet and stenosis respectively, and  $th3$  is the threshold of velocity. Otherwise, the average velocity of inlet and outlet is introduced to compute the rate of stenosis as  $P_s = 1 - \frac{V_{in} + V_{out}}{2V_s}$  because the simulated incompressible fluid must flow past the same area though inlet/outlet and stenosis.

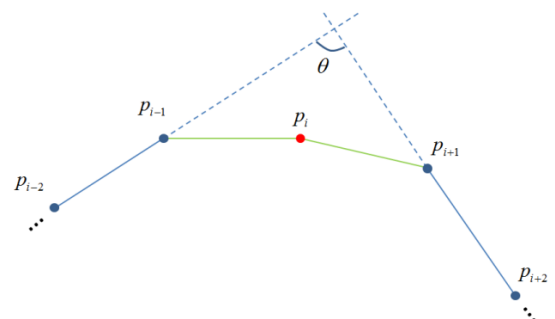


Fig. 7. Feature nodes optimization

**Step 5:** The generation of surgical path directed tree

From previous steps, we have constructed entire directed tree of blood vessel and marked the stenosis of the blood vessel. So we use the combined node of marked stenosis branch to determine the directed tree of surgical path, and other branches without stenosis are cut.

The nodes of surgical path directed tree generated by previous steps may be too dense in local. That will bring about the slower fitting speed and local fluctuation ap-

pearing on the fitting curve. So it needs to optimize these nodes before fitting the final surgical path.

In Fig.7,  $p_{i-2}, p_{i-1}, p_i, p_{i+1}$  and  $p_{i+2}$  ( $p_{i-1}, p_i$  and  $p_{i+1}$  are not the branch nodes) are the five continuous feature nodes with adjacent distance  $D_1, D_2, D_3$  and  $D_4$ , and the angle  $\theta$  is determined by the extended lines of  $\widehat{p_{i-2}p_{i-1}}$  and  $\widehat{p_{i+1}p_{i+2}}$ . If  $\theta > \text{Th1}$  ( $\text{Th1}$  is a threshold), the node  $p_i$  needs to be removed. If  $\text{dist}(p_{i-1}, p_i) < \text{Th2}$  ( $\text{Th2}$  is a threshold), the node  $p_i$  needs to be removed. If  $\text{Average}(D_1, D_2, D_3, D_4) < D_2$  or  $D_3$ , the node  $p_i$  does not need to be optimized.

#### Step 6: The surgical path fitting

Finally, we use the Catmull-Rom spline fitting method to get a smooth and single-pixel surgical path from optimized directed tree. And the final surgical path extraction result of Y-type pipe is shown in Fig.8.

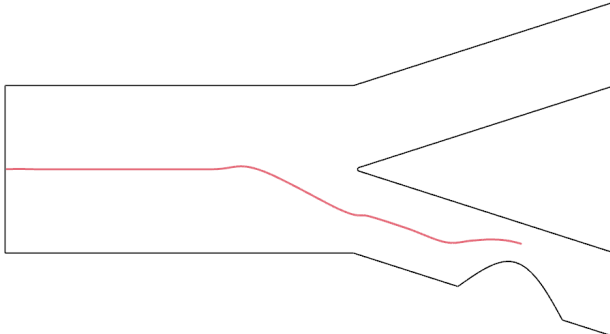


Fig. 8. Final surgical path

## IV. Validation

The surgical path consists of several centerlines at the leisure parts of blood vessels. To verify the correctness of our algorithm, we extract the centerline of two regular tubular structure (Y-type pipe and U-type pipe) and calculate the errors between the standard centerline and our results under different cases.

#### (1) Regular Y-type pipe structure

In this experiment, we extract the centerline of regular Y-type pipe, and compare and analyze the extraction accuracy error under different number of pressure level, as shown in Fig.9(1). Fig.9(1-a) shows the original extracted isobars result with 116 levels, Fig.9(1-b) shows the optimized isobars result and their corresponding center point, and Fig.9(1-c) shows the final fitting centerline.

**Table 1. The errors value of Y-type pipe**

Figure	(a)	(b)	(c)	(d)
Isobars number	116	58	29	14
Error-sum	19.985	22.338	26.492	34.834
Average Error	0.033	0.037	0.044	0.058

Next, we use different pressure levels to extract the centerline of regular Y-type pipe. And the error comparison results are shown in Fig.10(1): the red full line is the fitting centerline extracted by our algorithm, and the blue dotted line is the ground truth of centerline. In this experiment, the number of our fitting spline point is 600, and the errors under different pressure levels are indicated in Table 1, where Error-sum is the sum error of all spline point to the ground truth, and Average Error is average error of each spline point. From the results, we can see that the more pressure levels we divided, the higher precision of generated centerline we got.

Since we transferred the problem from 2d image to 2d virtual space, the error values in our paper are the position distance between the generated vertex position of centerline to the vertex position of the ground truth centerline. Moreover, the ground truth of centerlines in these regular vessels are directly obtained by hand other than by other methods because the centerlines of these regular pipes can be defined by hand without any error.

**Table 2. The errors value of U-type pipe**

Figure	(a)	(b)	(c)	(d)
Isobars number	145	72	36	18
Error-sum	6.578	6.689	7.783	9.853
Average Error	0.033	0.033	0.039	0.049

#### (2) Regular U-type pipe structure

The same as Y-type pipe experiment, our algorithm is applied in regular U-type pipe, as shown in Fig.9(2). And the error comparison results is shown in Fig.10(2). In this experiment, the number of our fitting spline point is 200 and the errors under different pressure levels are indicated in Table 2. From the results, we can draw the same conclusion as regular Y-type pipe, and furthermore, when reaching the certain pressure levels, the accuracy of centerline tends to be stable.

**Table 3. The errors value with optimization and non-optimization**

Figure	(a)	(b)	(c)	(d)
Pipe Structure	Y-type non-opt.	Y-type opt.	U-type non-opt.	U-type opt.
Isobars number	116	116	72	72
Error-sum	21.995	19.985	6.668	6.578
Average Error	0.037	0.033	0.034	0.033

#### (3) Optimization error comparison

We use the best centerline extraction result from previous experiments for accuracy comparison between optimization and non-optimization for directed tree. In this experiment, the pressure level number of regular Y-type pipe is 116, the U-type pipe is 72, and the extraction results are shown in Fig.11. Fig.11(a)(b) show the extraction results for Y-type pipe and U-type pipe respectively with non-optimization, that the centerline (red full line)

exists the problem of local oscillation. And Fig.11(c)(d) show the corresponding optimized results, that the optimized centerline is smoother. The errors comparison results between optimization and non-optimization are shown in Table 3. From the results, we can see that the centerline is more accurate and smoother after optimization.

#### (4) Rate of stenoses

The Y-type pipe in the above description (see Fig.5) is adopted to validate the accuracy of our method. In this experiment, the ground truth of stenosis rate is 50.0% and the rate of stenosis by our method is computed as

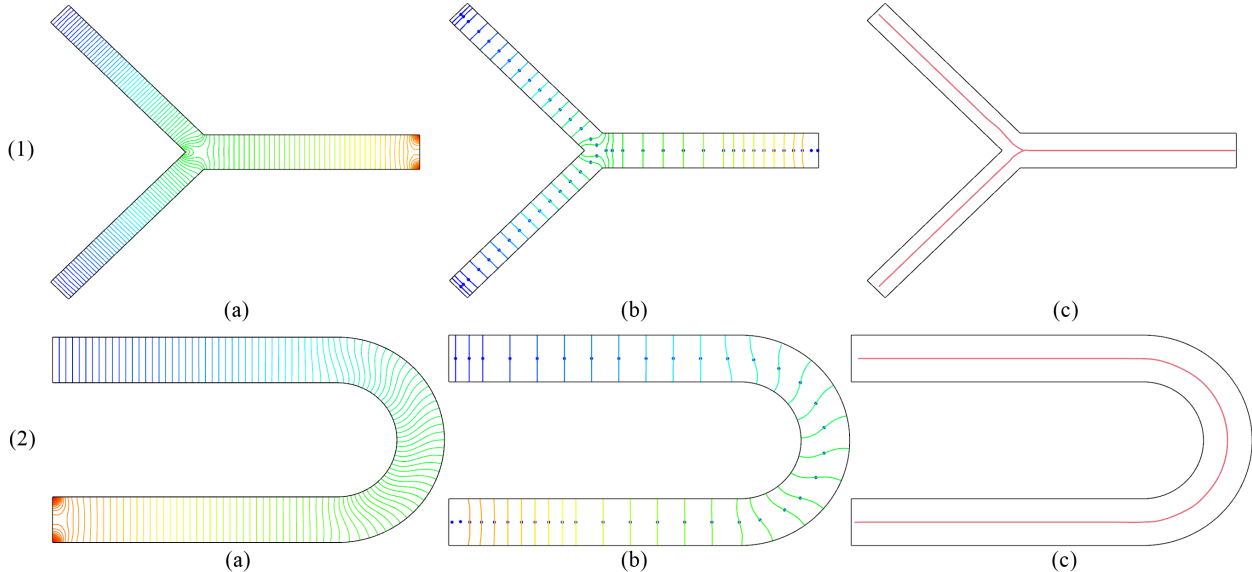


Fig. 9. Centerline extraction result of regular Y and U-type pipe

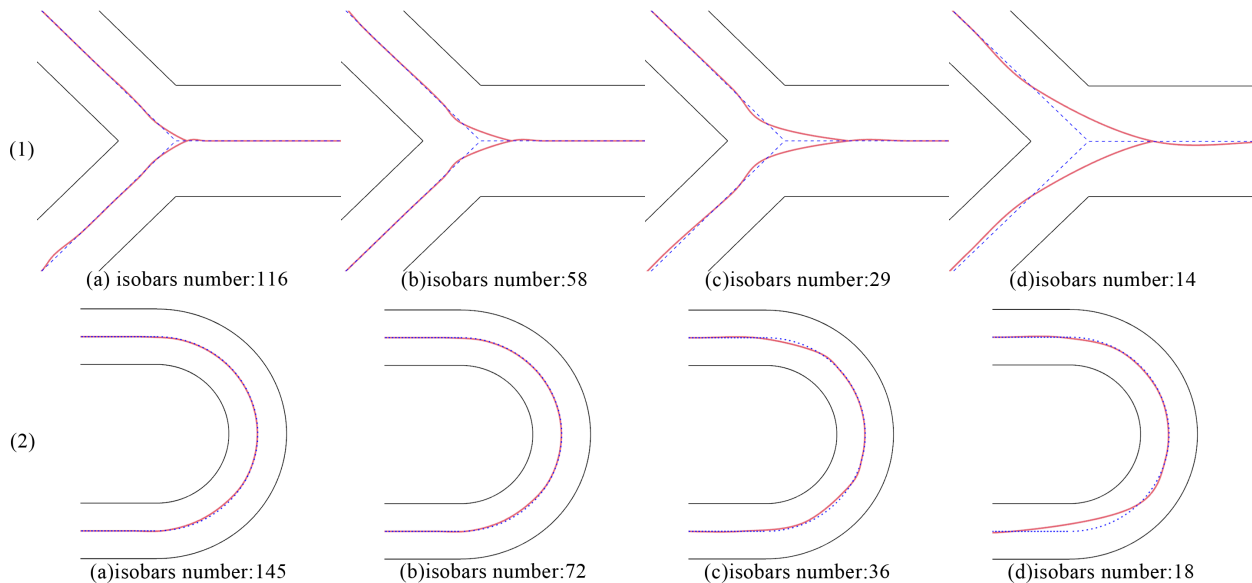


Fig. 10. Errors comparison with different pressure levels in Y and U-type pipe

47.3%. Since there is no node remain in the stenosis tree branch, the end node is choose as the outlet of stenosis. The corresponding all node velocities through the stenosis are shown in Fig.12, from this velocity data we can see the velocity at the end node is significantly larger than the inlet node, but within the threshold, which lead to inaccuracy of the result.

## V. Results

In this section, our path planning method is applied in the real angiography images to get the surgical path information with rate of stenosis analysis.

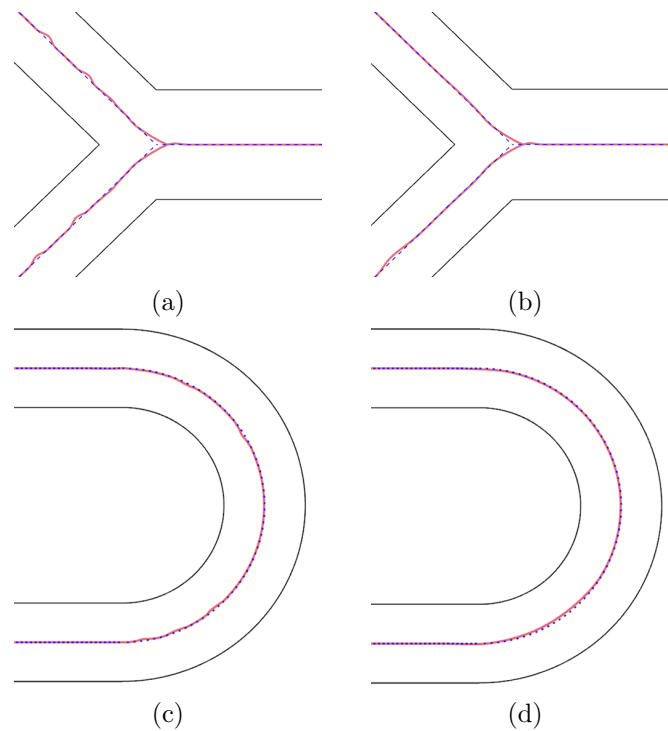


Fig. 11. Errors comparison between optimization and non-optimization

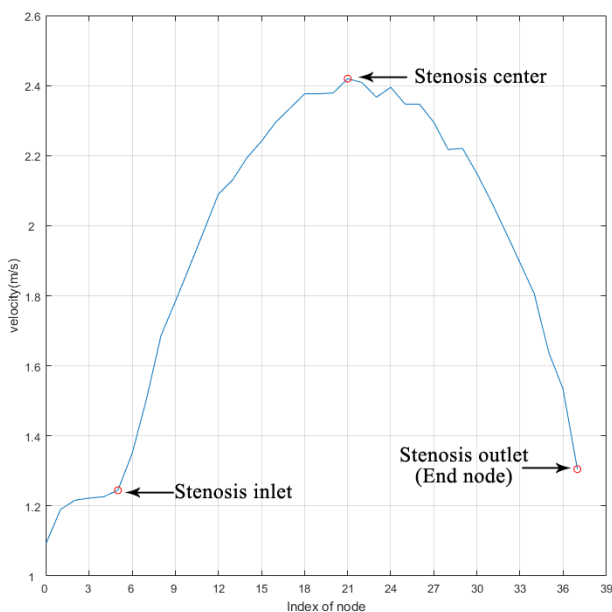


Fig. 12. Velocity of tree nodes through the stenosis

We design three types experiments to present the results of this algorithm, including single stenosis, multiple stenoses and no stenosis case, which are shown in Fig.13.

### (1) Single stenosis case

In this case, we extract the surgical path from the real coronary artery angiography image (seeing Fig.13(a)) with only one remarkable stenosis. After vessel segmentation, the path between surgical approach to stenosis is generated by our method and drawn in the medical image in red, shown in Fig. 13(b). In additional, the information of the rate of stenosis is marked in the image too for the further analysis. From the result, we can see that the surgical path is a smooth and one-pixel curve, whose position is in consonance with the center perceived by human vision.

### (2) Multiple stenoses case

Different from the above case, we use the angiography image with remarkable stenoses (seeing Fig.13(c)) to test the accuracy of our method. As shown in Fig.13(d), four remarkable stenoses are detected and marked with their rates in the image, and the final path are represented in red line. From the result, all stenoses are obtained accurately and the final surgical path is start from the surgical approach to the final stenosis.

### (3) No stenosis case

In the third experiment, the angiography image, captured from healthy human, is used in our method. Because there are not any stenoses inside the blood vessels, our method adopts the positions of presetting outlets as end points of path. Therefore, the centerline of the vessel is extracted as the final path, which is shown in Fig.13(g).

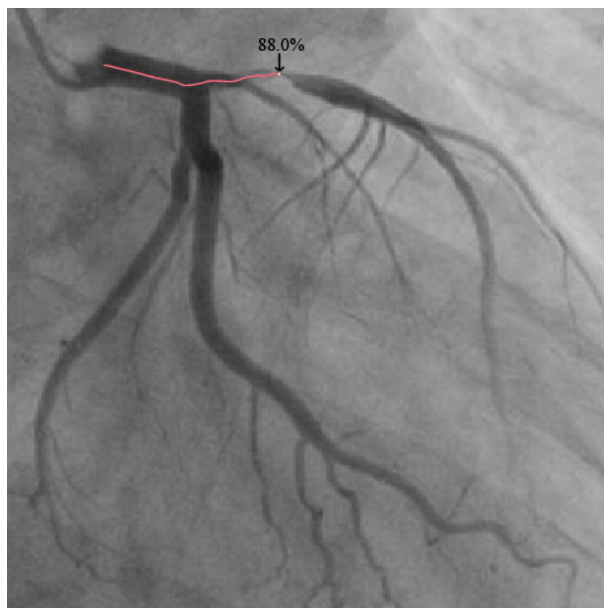
The experimental hardware is a computer with Intel(R) Core(TM) i7-6820HK@2.70GHz and 8GB memory and the performance of above experiments is shown in Table 4. Since the Meandering Triangle method needs to meander every triangles to obtain every isoline and assemble the extracted lines into isobars, the computation cost of isobars extraction is most time consuming step which related to the number of Delaunay triangles. After obtained every isobar, the cost of directed tree construction is determined by the complexity of the vessel and thus it is harder to generate the original structure of single stenosis and multiple stenoses case than no stenosis one. Then, stenosis detection step is applied to the original directed tree to cut the branches of healthy part. Since the structure of no stenosis is simple and there is no stenosis, it processes fast. Finally, the surgical path is fast fitted by the Catmull-Rom spline fitting method.

**Table 4. The performance of our path planning method**

Experiment	(1)single stenosis case	(2) multiple stenoses case	(3) No stenosis case
Isobars extraction	9.812s	12.926s	8.907s
Directed tree construction	0.152s	0.169s	0.107s
Stenosis detection	0.921s	1.151s	0.019s
Path generation	0.001s	0.002s	0.005s



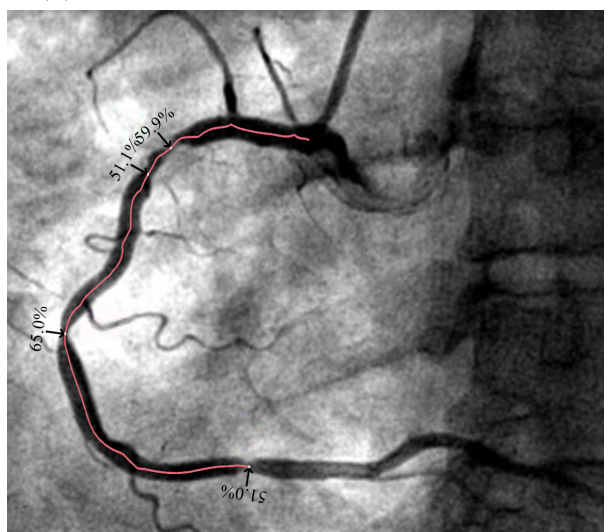
(a) Single stenosis case



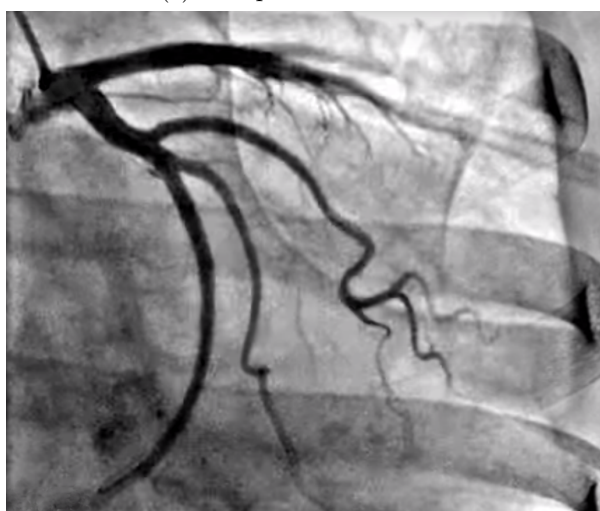
(b) Path planning result of single stenosis case



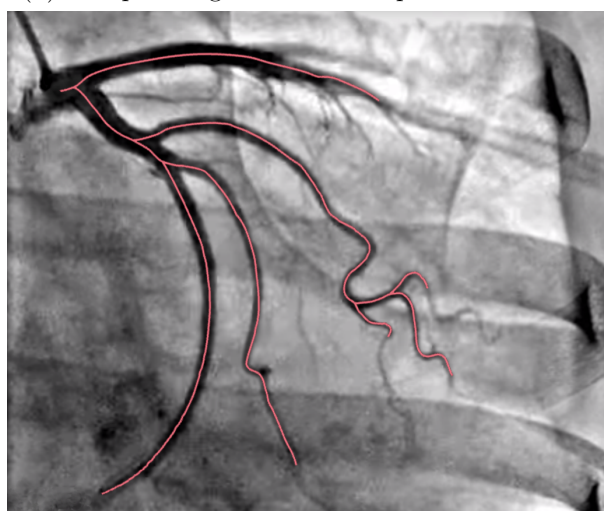
(c) Multiple stenoses case



(d) Path planning result of multiple stenoses case



(e) No stenosis case



(f) Path planning result of no stenosis case

Fig. 13. Path planning results for real angiography images

## VI. Conclusion

This paper presents a novel path planning method based on steady fluid dynamics for minimally invasive vascular surgery with less interventions and high accuracy. At the step of vessel segmentation, Graph-cuts theory was used to model vessel structures and obtain the accurate boundary information of the coronary angiography images. At the step of isobars extraction, a set of isobars in blood vessels was obtained by FVM and Meandering Triangles algorithm when blood flowing steadily. At the step of surgical path generation, the directed vessels-tree with flow velocity was constructed for the stenoses detection, and the final smooth and single-pixel surgical path was fitted.

In the future work, we will improve the algorithm and expand it to 3D vascular structures, and implement a system for the planning and true guidance of minimally invasive vascular surgery.

## References

- [1] A. Hernandez-Vela, C. Gatta, S. Escalera, et al., “Accurate Coronary Centerline Extraction, Caliber Estimation, and Catheter Detection in Angiographies”, *IEEE Transactions on Information Technology in Biomedicine*, Vol.16, No.6, pp.1332–1340, 2012.
- [2] H. Blum, “Models for the perception of speech and visual form”, *MIT press*, USA, pp.362–380, 1967.
- [3] Z. Shoujun, Y. Jian, W. Yongtian, C. Wufan, “Automatic segmentation of coronary angiograms based on fuzzy inferring and probabilistic tracking”, *Biomedical engineering online*, Vol.9, No.40, pp.1–21, 2010.
- [4] I. Cruz-Aceves, F. Oloumi, RM. Rangayyan, et al., “Automatic segmentation of coronary arteries using Gabor filters and thresholding based on multiobjective optimization”, *Biomedical Signal Processing and Control*, Vol.25, pp.76–85, 2016.
- [5] K. Krissian, G. Malandain, N. Ayache, et al., “Model based detection of tubular structures in 3d images”. *Computer vision and image understanding*, Vol.80, No.2, pp.130–171, 2000.
- [6] J. Staal, MD. Abràmoff, M. Niemeijer, et al., “Ridge-based vessel segmentation in color images of the retina”, *IEEE Transactions on medical imaging*, Vol.23, No.4, pp.501–509, 2004.
- [7] OKC. Au, CL. Tai, HK. Chu, et al., “Skeleton extraction by mesh contraction”, *ACM Transactions on Graphics (TOG)*, Vol.27, No.3, pp.1567–1573, 2008.
- [8] S. Wang, J. Wu, M. Wei, X. Ma, “Robust curve skeleton extraction for vascular structures”, *Graphical Models*, Vol.74, No.4, pp.109–120, 2012.
- [9] J. Wu, H. Wang, P. Zhang, et al., “A preliminary real-time and realistic simulation environment for percutaneous coronary intervention”, *BioMed research international*, 183157:10, 2015.
- [10] B. Liu, AC. Telea, JBTM. Roerdink, et al. “Parallel centerline extraction on the gpu”, *Computers & Graphics*, Vol.41, No.1, pp.72–83, 2014.
- [11] D. Jin, KS. Iyer, C. Cheng, et al., “A robust and efficient curve skeletonization algorithm for tree-like objects using minimum cost paths”, *Pattern Recognition Letters*, Vol.76, pp.32–40, 2015.
- [12] N. Mayya, VT. Rajan, “An efficient shape representation scheme using voronoi skeletons”, *Pattern Recognition Letters*, Vol.16, No.2, pp.147–160, 1995.
- [13] JF. Fan, Y. Jian, YT. Wang, “A fast vascular centerline extraction method based on voronoi diagram” *Beijing Ligong Daxue Xuebao/transaction of Beijing Institute of Technology*, Vol.33, No.12, pp.1303–1308, 2013.
- [14] F. Yang, ZG. Hou, SH. Mi, et al., “Centerlines extraction for lumen model of human vasculature for computer-aided simulation of intravascular procedures”, *Intelligent Control and Automation*, pp.970–975, 2014.
- [15] AP. Kiraly, JP. Helferty, EA. Hoffman, G. McLennan, “Three dimensional path planning for virtual bronchoscopy”, *IEEE Transactions on Medical Imaging*, Vol.23, No.11, pp.1365C79, 2004.
- [16] DG. Kang, JB. Ra, “A new path planning algorithm for maximizing visibility in computed tomography colonography”, *IEEE Transactions on Medical Imaging*, Vol.24, No.8, pp.957–968, 2005.
- [17] Y. Xu, G. Liang, G. Hu, et al., “Quantification of coronary arterial stenoses in cta using fuzzy distance transform”, *Computerized Medical Imaging and Graphics*, Vol.36, No.1, pp.11–24, 2012.
- [18] A. Eslami, A. Aboee, Z. Hodaei, et al., “Quantification of coronary arterial stenosis by inflating tubes in ct angiographic images”. *Proc. MICCAI Workshop 3D cardiovascular imaging: a MICCAI segmentation challenge*, 2012.
- [19] K. Mori, J. Hasegawa, Y. Suenaga, J. Toriwaki. “Automated anatomical labeling of the bronchial branch and its application to the virtual bronchoscopy system”, *IEEE Transactions on Medical Imaging*, Vol.19, No.2, pp.103–114, 2000.
- [20] J. Tschirren, G. McLennan, K. Palcgyi, et al., “Matching and anatomical labeling of human airway tree”, *IEEE Transactions on Medical Imaging*, Vol.24, No.12, pp.1540–1547, 2005.
- [21] R. Zwigelaar, SM. Astley, CR. Boggis, CJ. Taylor, “Linear structures in mammographic images: detection and classification”, *IEEE Transactions on Medical Imaging*, Vol.23, No.23, pp.1077–1086, 2004.
- [22] PK. Saha, Y. Xu, H. Duan, A. Heiner, G. Liang, “Volumetric topological analysis: a novel approach for trabecular bone classification on the continuum between plates and rods”, *IEEE Transactions on Medical Imaging*, Vol.29, No.29, pp.1821C1838, 2010.
- [23] P. Li, S. Jiang, D. Liang, et al., “Modeling of path planning and needle steering with path tracking in anatomical soft tissues for minimally invasive surgery”, *Medical Engineering & Physics*, Vol.41, pp.35–45, 2017.
- [24] L. Mei, Z. Ke, “The influence of arterial stenosis in bifurcate blood vessel on the blood flow”, *Chinese Journal of Applied Mechanics*, Vol.3, pp.417–421, 2013.